J Biomol NMR (2012) 54:325–335
DOI 10.1007/s10858-012-9680-z

COMMUNICATION

Solid state NMR of proteins at high MAS frequencies: symmetry-based mixing and simultaneous acquisition of chemical shift correlation spectra

Peter Bellstedt · Christian Herbst · Sabine Häfner · Jörg Leppert · Matthias Görlach · Ramadurai Ramachandran

Received: 18 September 2012 / Accepted: 29 October 2012 / Published online: 23 November 2012

Abstract We have carried out chemical shift correlation experiments with symmetry-based mixing sequences at high MAS frequencies and examined different strategies to simultaneously acquire 3D correlation spectra that are commonly required in the structural studies of proteins. The potential of numerically optimised symmetry-based mixing sequences and the simultaneous recording of chemical shift correlation spectra such as: 3D NCAC and 3D NHH with dual receivers, 3D NC′C and 3D C′NCA with sequential ^{13}C acquisitions, 3D NHH and 3D NC′H with sequential ^{1}H acquisitions and 3D CANH and 3D C'NH with broadband ^{13}C–^{15}N mixing are demonstrated using microcrystalline samples of the β1 immunoglobulin binding domain of protein G (GB1) and the chicken α-spectrin SH3 domain.

Keywords Solid state NMR · Magic angle spinning · Symmetry-based mixing · Dual receivers · Chemical shift correlation

Introduction

Multi-dimensional chemical shift correlation experiments with mixing periods leading to ^{15}N–^{13}C and ^{13}C–^{13}C dipolar and scalar coupling mediated magnetisation transfers, both band-selective and broadband, are performed in MAS solid state NMR studies of proteins (Kehlet et al. 2007; Franks et al. 2007; Chen et al. 2007; Nielsen et al. 2009; Loening et al. 2012). Although weak dipolar couplings between low γ nuclei are typically averaged out under magic angle spinning (MAS) conditions, the spatial averaging of weak dipolar interactions can be inhibited via the application of suitable RF pulse sequences. The CN_n^ν and RN_n^ν symmetry-based approach (Levitt 2002) provides a general framework for the design of different homo- and heteronuclear mixing sequences and has found a variety of applications in biomolecular MAS solid state NMR studies. The CN_n^ν class of RF pulse schemes involves the application of a basic element "*C*", corresponding to an RF cycle with unity propagator U_{RF} (t_c) = 1, *N* times over *n* rotor periods τ_r with successive *C* elements incremented in phase by $\nu 2\pi/N$. RF pulse sequences belonging to RN_n^ν symmetry involve the application of the pulse sandwich $\{R\varphi R\text{-}\varphi\}$, where $\varphi = \pi\nu/N$ and *R* is a 180° pulse, *N*/2 times over *n* rotor periods so as to form an RF cycle with unity propagator U_{RF} (t_c) = 1. *N*, *n* and ν are all integers and appropriate values for these are chosen, via the selection rule for CN_n^ν and RN_n^ν symmetry, to generate the desired average Hamiltonian. One of the difficulties with the symmetry-based RF pulse schemes based on conventional composite RF pulses, however, is that the RF field strength requirements are related to the spinning speed. This may lead to situations where the RF field strength needed becomes too large, thus limiting its applicability at high MAS frequencies that are typically employed to minimise the effects of CSA at high Zeeman field strengths and in experiments involving direct proton detection. As a result, most of the biomolecular NMR studies involving symmetry-based mixing sequences reported till date have been

Electronic supplementary material The online version of this article (doi:10.1007/s10858-012-9680-z) contains supplementary material, which is available to authorized users.

P. Bellstedt · S. Häfner · J. Leppert · M. Görlach · R. Ramachandran (✉)
Biomolecular NMR spectroscopy, Leibniz Institute for Age Research, Fritz Lipmann Institute, 07745 Jena, Germany
e-mail: raman@fli-leibniz.de

C. Herbst
Department of Physics, Faculty of Science, Ubon Ratchathani University, Ubon Ratchathani 34190, Thailand

carried out essentially at moderate MAS frequencies. To overcome this problem, we have developed a numerical approach for the design of efficient symmetry-based mixing schemes (Herbst et al. 2009a, b, c, 2010, 2011) taking into account experimental requirements and constraints, e.g. MAS frequency and RF field strength. This exploits the fact that for the recoupling and decoupling of different nuclear spin interactions the symmetry-based approach provides a large number of inequivalent symmetries involving the application of basic "*R*"/"*C*" elements of different durations. Our studies have demonstrated that the design of mixing sequences via the symmetry-based approach is neither restricted to broadband mixing nor to moderate MAS frequencies. By selecting appropriate symmetries and optimising the RF field modulation profile of the basic elements, it is equally possible to implement both high-power broadband and low-power band-selective mixing sequences for any desired MAS frequency. Here, we have carried out, homo- and heteronuclear chemical shift correlation experiments at different MAS frequencies and Zeeman field strengths using microcrystalline samples of the β1 immunoglobulin binding domain of protein G (GB1) (Zhou et al. 2007; Franks et al. 2007) and the chicken α-spectrin SH3 domain (Castellani et al. 2003; Akbey et al. 2010; Linser et al. 2011), in their protonated as well as perdeuterated form. Different strategies to achieve simultaneous acquisition of chemical shift correlation spectra that are commonly required in protein MAS NMR investigations have been examined. We show that it is possible to effectively employ numerically optimised symmetry-based mixing sequences in protein solid state NMR at high MAS frequencies and to achieve *simultaneous* acquisition of chemical shift correlation spectra 3D NCAC and 3D NHH using dual receivers, 3D NC′C and 3D C′NCA employing *sequential* acquisitions with a single receiver, 3D NHH and 3D NC′H with *sequential* ^{1}H acquisitions and 3D CANH and 3D C′NH with broadband ^{13}C–^{15}N mixing sequences.

Materials and methods

Sample preparation

Uniformly (^{13}C–^{15}N) labelled microcrystalline samples of GB1 and the SH3 domain were used in these studies. The T3Q mutant of GB1 was expressed, purified and crystallized based on a published protocol (Franks et al. 2005). Protein expression in M9 media containing 1 g/l $^{15}NH_4Cl$ and 2 g/l ^{13}C-glucose or 2 g/l [^{13}C, ^{2}H]-glucose for perdeuterated sample was induced with 0.3 mM isopropyl ß-D-thiogalactoside for 3 h at 310 K. A 5 mg/ml solution of purified GB1 in 50 mM KH_2PO_4/K_2HPO_4 was used for precipitation, microcrystals were collected by centrifugation after 1 day at room temperature and packed into a 2.5 mm rotor, which was sealed with silicone disks to minimize sample dehydration during the experiments. In case of the perdeuterated GB1 sample partial back-exchange of labile protons was achieved by dissolving lyophylized GB1 in a D_20/H_20 mixture (ratio 90:10) and incubation at 323 K for 6 h prior to crystallization. Traces of NaCl through incomplete dialysis resulted in an alternative microcrystalline form of GB1 (Frericks Schmidt et al. 2007) and is referred to as crystal form B here. Perdeuterated SH3 was expressed identically to GB1 except that the M9 media contained 1.5 g/l [^{13}C, ^{2}H]-glucose. Cells were disrupted using a french press, debris was removed by centrifugation (16,000×*g*, 277 K, 30 min) and supernatant was subjected to an anion exchange chromatography (DEAE Sepharose). The flow-through was collected and a subsequent ultracentrifugation step (50,000×*g*, 277 K, 30 min) was used to remove unwanted high molecular weight proteins/aggregates prior to size exclusion chromatography (Sephadex 75). SH3 containing fractions were combined and dialysed 2 times against 4 l 10 mM sodium citrate pH 3.5, concentrated to 10 mg/ml, lyophylized, redisolved in D_2O/H_20 mixture (ratio 70:30) and incubated at 298 K overnight to partially back-exchange the amide protons. Crystallisation was initialized by changing the pH from 3.5 to ~7.5 by stepwise addition of NH_4OH solution. Microcrystals were collected after at least 3 days of incubation at 293 K by centrifugation and packed into a 2.5 mm rotor, which was sealed with silicone discs. Approximately 10–15 mg of protein was used to pack the rotors. Although the two microcrystalline forms of GB1 lead to slightly different spectral patterns, correlation spectra of high quality with good ^{15}N and ^{13}C spectral resolution could be generated with both samples.

NMR experiments

Multi-dimensional chemical shift correlation experiments were carried out at different MAS frequencies with either a Bruker 500 MHz wide-bore or a 750 MHz narrow-bore Avance III solid state NMR spectrometer equipped with 2.5 mm triple resonance probes and with the cooling air kept at a temperature such that the sample temperature corresponded to ~288 K. The numerically optimised symmetry-based mixing schemes reported recently (Herbst et al. 2009a, b, c, 2010, 2011) were used with appropriate scaling of the RF field strength and duration of the basic elements, where required. Unless indicated otherwise all spectra were collected with simultaneous ^{1}H decoupling during mixing. Phase sensitive chemical shift correlation spectra were generated by the States procedure (States et al. 1982). Standard phase cycling procedures were employed to select signals arising from desired coherence transfer pathways.

Results and discussion

One of the critical steps in multidimensional protein MAS solid state NMR experiments such as the 3D NCACX, NCOCX, CONCA and CONH is the magnetisation transfer between the backbone amide nitrogens and the ^{13}CA or ^{13}CO nuclei, respectively. Considering a resonance offset range of ±2 kHz and ^{13}C and ^{15}N RF field strengths of 10 kHz, optimised sequences such as $R16_{49}^{-5,4}$ and $R16_{63}^{-4,5}$ leading to ^{15}N–^{13}C γ-encoded heteronuclear double-quantum dipolar recoupling with suppression of chemical shift anisotropies and homonuclear dipolar coupling terms have been reported recently at MAS frequencies of 15 and 20 kHz, respectively (Herbst et al. 2011). Although designed for a specific MAS frequency, one of the advantages with our numerically optimised mixing sequences, in general, is the possibility to apply them to other MAS frequencies via appropriate scaling of the RF field strength and duration of the basic elements involved. The scalability and the efficacy of the optimised symmetry $R16_{49}^{-5,4}$ for band-selective mixing is demonstrated by 2D ^{15}N–^{13}CA and ^{15}N–^{13}CO correlation experiments using GB1 (Fig. 1a, b) collected at 750 MHz at a spinning speed of 27.5 kHz. ^{15}N → ^{13}C longitudinal magnetisation exchange was achieved using the $R16_{49}^{-5,4}$ symmetry with the corresponding scaled basic "*R*" elements of 111.36 μs duration and ^{13}C and ^{15}N RF field strengths of ∼18.3 kHz. As the ^{1}H decoupling field strength of ∼125 kHz used was still significantly larger than the recoupling RF field strengths, correlation spectra with good cross-peak intensities were observed due to minimal RF field interference effects during mixing. The crosspeak patterns are consistent with that reported for GB1 (Franks et al. 2007). The $R16_{49}^{-5,4}$ symmetry also yields satisfactory spectra at MAS frequencies of 20 and 33.333 kHz (supplementary Figs. 1, 2). Small variations in the ^{13}C and ^{15}N RF field strengths were not found to have any significant effect on the observed ^{15}N → ^{13}C magnetisation transfer characteristics (supplementary Fig. 3); i.e. the performance of the numerically optimised symmetries are expected to be unaffected by minor RF field inhomogeneities (±5 %). In addition to heteronuclear mixing, the performance of different optimised band-selective homonuclear mixing sequences were also experimentally evaluated. Optimised symmetry-based RF pulse schemes such as the $C7_{30}^{1}$ and $C9_{69}^{1}$ (Herbst et al. 2011) also work effectively at high MAS frequencies for obtaining dipolar and scalar coupling mediated ^{13}C–^{13}C correlation spectra, respectively, in the aliphatic region of proteins (supplementary Fig. 4).

Where sensitivity and resolution are favourable, the use of broadband mixing sequences leading to simultaneous magnetisation transfers from ^{15}N to both the ^{13}CA and ^{13}CO nuclei in a 3D NCC experiment may facilitate sequential resonance assignments using a single

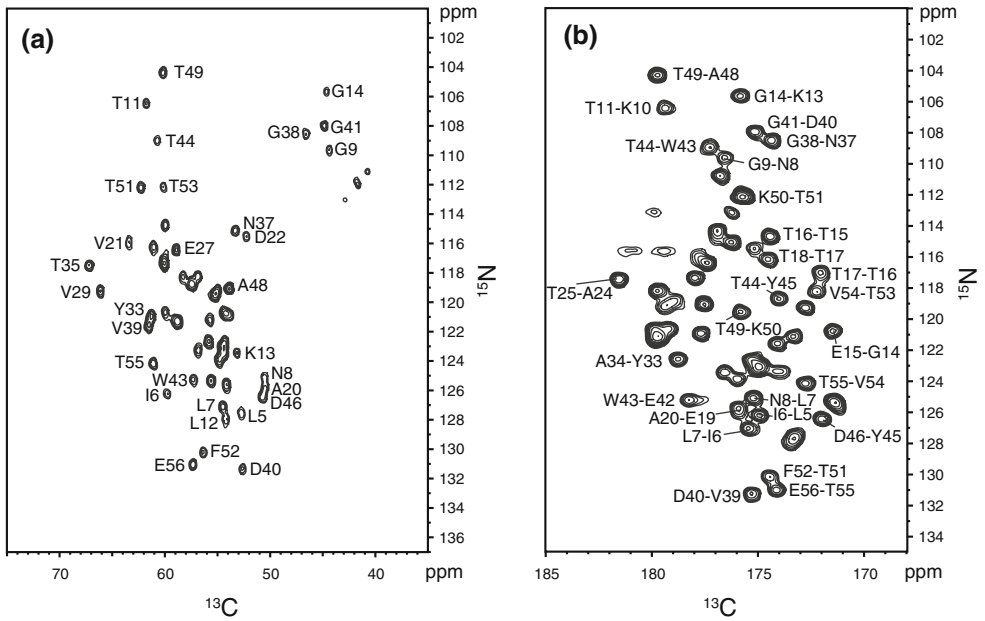

Fig. 1 (**a**) 2D ^{15}N–^{13}CA and (**b**)^{15}N–^{13}C' band-selective chemical shift correlation spectra of GB1 (crystal form A) recorded at 750 MHz and a spinning speed of 27.5 kHz. The $R16_{49}^{-5,4}$ symmetry with the corresponding numerically optimised (scaled) *R* elements reported earlier (Herbst et al. 2011), a CP contact time of 0.5 ms, τ_{mix} of 3.56 ms, ^{13}C and ^{15}N mixing RF field strengths of ∼18 kHz, 16 transients per t_1 increment, 80 t_1 increments, spectral width in the indirect dimension of 3,000 Hz and a recycle time of 2.0 s were used, keeping the ^{13}C RF carrier at 55 ppm (**a**) and 175 ppm (**b**) and the ^{15}N RF carrier at 120 ppm. Assignments are taken from the literature (Franks et al. 2007)

experiment by providing information about both the intra and inter-residue carbon chemical shifts. However, due to the large isotropic chemical shift separation between the ^{13}CA and ^{13}CO nuclei, large ^{13}C RF field strengths would typically be required to achieve efficient broadband mixing. This could lead to substantial signal losses in situations where the ^{15}N–^{13}C mixing is carried out in the presence of ^{1}H decoupling. However, in the study of perdeuterated samples at high MAS frequencies, efficient homo- and heteronuclear mixing can be carried out in the absence of ^{1}H decoupling (Huang et al. 2011; Knight et al. 2011). To achieve broadband mixing we have used a symmetry-based heteronuclear sequence (Brinkmann and Levitt 2001) designed for a simple ^{15}N–^{13}C two spin system. Figure. 2 shows the 2D ^{15}N–^{13}C broadband correlation spectrum of perdeuterated GB1 (NH:ND 10:90) acquired at 500 MHz and a spinning speed of 20 kHz using ^{15}N and ^{13}C recoupling RF field strengths of 44 kHz. The optimised symmetry $R24_{22}^{-5,7}$, designed (Herbst et al. 2009c) considering a resonance offset range of ±8 and ±2 kHz for the ^{13}C and ^{15}N nuclei, respectively, was employed. The ^{15}N–^{13}CA and ^{15}N–^{13}CO correlation peak patterns observed matches with that obtained via band-selective mixing sequences. It is also worth pointing that efficient broadband ^{15}N–^{13}C mixing can be realised with only moderate ^{15}N and ^{13}C RF field strengths. In addition to ^{15}N–^{13}C mixing, mixing periods leading to ^{13}C–^{13}C magnetisation transfers constitute another critical building block in many of the multi-dimensional chemical shift correlation experiments that are performed in the study of proteins. ^{13}C–^{13}C broadband mixing can be conveniently implemented via different proton driven spin diffusion based mixing schemes (Hou et al. 2010). However, in a variety of situations active dipolar recoupling schemes would be required; e.g. in double-quantum spectroscopy. In this context, the performance of different optimised broadband ^{13}C–^{13}C double-quantum dipolar recoupling sequences, such as $R16_{14}^{-7}$ and $C8_{10}^{3}$ reported recently (Herbst et al. 2009b, c), were also experimentally evaluated at high MAS frequencies and found to lead to correlation spectra of high quality (supplementary Fig. 5). Although symmetry-based mixing sequences have not been widely applied for protein solid state NMR studies at high MAS frequencies, the data presented here demonstrate the potential of our numerically optimised symmetry-based mixing sequences in such investigations.

Although the RF pulse schemes reported here can lead to efficient mixing, these symmetry-based mixing schemes do not lead to *complete* magnetisation transfers (Levitt 2002). Hence, sensitivity permitting, it is possible to effectively use also the *residual* magnetisation and achieve simultaneous acquisition of signals arising via different magnetisation transfer pathways of interest. For example,

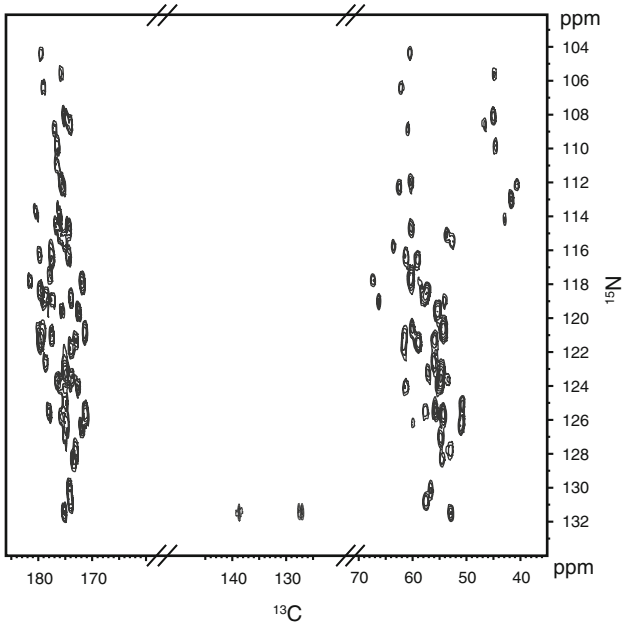

Fig. 2 2D ^{15}N–^{13}C broadband chemical shift correlation spectrum of perdeuterated GB1 (crystal form A) recorded at 500 MHz and a spinning speed of 20 kHz without ^{1}H decoupling during mixing. The $R24_{22}^{-5,7}$ symmetry with the corresponding numerically optimised *R* element reported earlier (Herbst et al. 2010, Fig. S2), a CP contact time of 2 ms, τ_{mix} of 2.2 ms, ^{13}C and ^{15}N mixing RF field strengths of 44 kHz, 512 transients per t_1 increment, 48 t_1 increments, spectral width in the indirect dimension of 2,027 Hz and a recycle time of 2.0 s were used, keeping the ^{13}C and ^{15}N RF carriers, respectively, at 115 and 120 ppm

with dual receivers, the RF pulse scheme given in Fig. 3a permits the one shot acquisition of 3D NCAC (Castellani et al. 2003; Franks et al. 2007; Schuetz et al. 2010; Sperling et al. 2010; Shi et al. 2011; Habenstein et al. 2011) and 3D NHH (Paulson et al. 2003; Zhou et al. 2007; Linser et al. 2011) correlation spectra. In this scheme, the initial transverse ^{15}N magnetisation generated by the first cross-polarisation (CP) step is allowed to evolve during the t_1/t_1' period. The magnetisation at the end of the evolution period is flipped to the *z* axis and then subjected to a period of ^{15}N → ^{13}CA longitudinal magnetisation exchange via the application of a band-selective mixing sequence. The ^{13}C polarisation generated at the end of the heteronuclear mixing period is brought to the transverse plane and allowed to evolve during the t_2 period. The ^{13}C magnetisation at the end of t_2 is then flipped to the *z* axis and subjected to longitudinal homonuclear mixing during the period τ_{mix}^{CC}. The magnetisation at the end of τ_{mix}^{CC} is rotated back to the transverse plane and detected in t_3 to generate the 3D NCAC spectrum. After the completion of the acquisition of the ^{13}C FID, proton saturation pulses with alternating *x* and *y* phases were first applied for 200 ms at a power level of ~25 kHz to achieve water suppression (Zhou and Rienstra 2008) and then the *residual* ^{15}N

longitudinal magnetisation remaining after the first $^{15}N \rightarrow {}^{13}CA$ transfer step is brought to the transverse plane and subjected to a CP step for transferring the t_1' modulated ^{15}N magnetisation to the directly attached proton. The proton magnetisation is allowed to evolve during the t_2' period and then flipped to the z axis. Longitudinal magnetisation exchange mediated by proton–proton dipolar couplings is allowed to take place during the mixing period τ_{mix}^{HH}. The proton magnetisation at the end of τ_{mix}^{HH} is rotated back to the transverse plane for direct detection in t_3' to generate the 3D NHH spectrum that provides information about proton–proton spatial proximities. With this approach using the optimised $R16_{49}^{-5,4}$ symmetry-based band-selective heteronuclear mixing scheme, we have succesfully acquired the 3D NCAC and NHH spectra of a perdeuterated sample of GB1 (Fig. 4) using RFDR (Bennett et al. 1998; Brinkmann et al. 2002; Leppert et al. 2003) during τ_{mix}^{HH} and τ_{mix}^{CC}.

While exploiting dual receiver capabilities is one way of achieving simultaneous acquisition of 3D correlation spectra of proteins in the solid state, an alternative approach to simultaneous data collection with a single receiver involves the use of sequential acquisition procedure reported recently (Gopinath and Veglia 2012a, b). For example, the RF pulse scheme shown in Fig. 3b, involving dual sequential proton detection, permits the simultaneous acquisition of 3D NCOH and NHH chemical shift correlation spectra. These spectra resulting from the magnetisation transfer pathways $^1H_N \rightarrow {}^{15}N \rightarrow {}^{13}CO \rightarrow {}^1H_N$ and $^1H_N \rightarrow {}^{15}N \rightarrow {}^1H_N \leftrightarrow {}^1H_N$, respectively, provide information about CO $\leftrightarrow$ H_N (Agarwal et al. 2010; Linser 2012) and $H_N \leftrightarrow H_N$ (Paulson et al. 2003; Zhou et al. 2007; Linser et al. 2011) spatial proximities. In this scheme, the initial transverse ^{15}N magnetisation generated by the first cross-polarisation (CP) step is allowed to evolve during the t_1/t_1' period. The magnetisation at the end of the evolution period is flipped to the z axis and then subjected to a period of $^{15}N \rightarrow {}^{13}CO$ longitudinal magnetisation exchange via the application of a band-selective mixing sequence. The ^{13}C polarisation generated at the end of the heteronuclear mixing period is brought to the transverse plane and allowed to evolve during the t_2' period. Homonuclear decoupling during ^{13}CO evolution was achieved via the application of a sandwich of pulses and delays $\{t2'/2 - (180)^{CA} - t2'/2 - (180) - \Delta\}$ with the delay Δ set to the duration of the band-selective $(180)^{CA}$ pulse. The ^{13}CO magnetisation at the end of t_2' is then flipped to the z axis and proton saturation pulses with alternating x and y phases were first applied for 200 ms at a power level of $\sim$25 kHz to achieve water suppression (Zhou and Rienstra 2008). The *residual* ^{15}N longitudinal magnetisation remaining after the first $^{15}N \rightarrow {}^{13}CO$ transfer step is brought to the transverse plane and subjected to a CP step for transferring

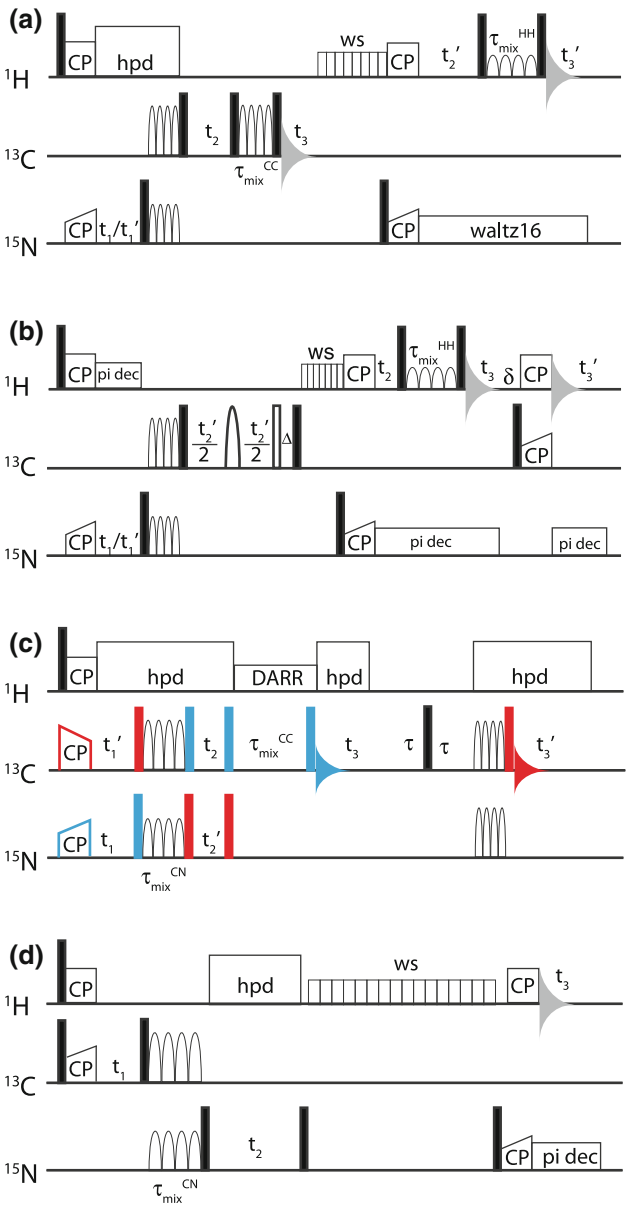

Fig. 3 RF pulse schemes for the simultaneous acquisition of (**a**) 3D NCAC and 3D NHH (**b**) 3D NCOH and 3D NHH **c** 3D NC'C (in *blue*) and 3D C'NC (in *red*) and **d** 3D CANH and 3D C'NH chemical shift correlation spectra with dual receivers (**a**), dual sequential acquisition in the direct dimension (**b**,**c**) and broadband ^{13}C–^{15}N mixing (**d**). Open and filled *rectangles* represent 180° and 90° pulses, respectively

the t_1 modulated ^{15}N magnetisation to the directly attached proton. The proton magnetisation is allowed to evolve during the t_2 period and then flipped to the z axis. Longitudinal magnetisation exchange mediated by proton–proton dipolar couplings is allowed to take place during the mixing period τ_{mix}^{HH}. The proton magnetisation at the end of τ_{mix}^{HH} is rotated back to the transverse plane for direct detection in t_3 to generate the 3D NHH spectrum. After the completion of the first ^1H acquisition and after a short delay, the ^{13}CO magnetisation is brought to the transverse

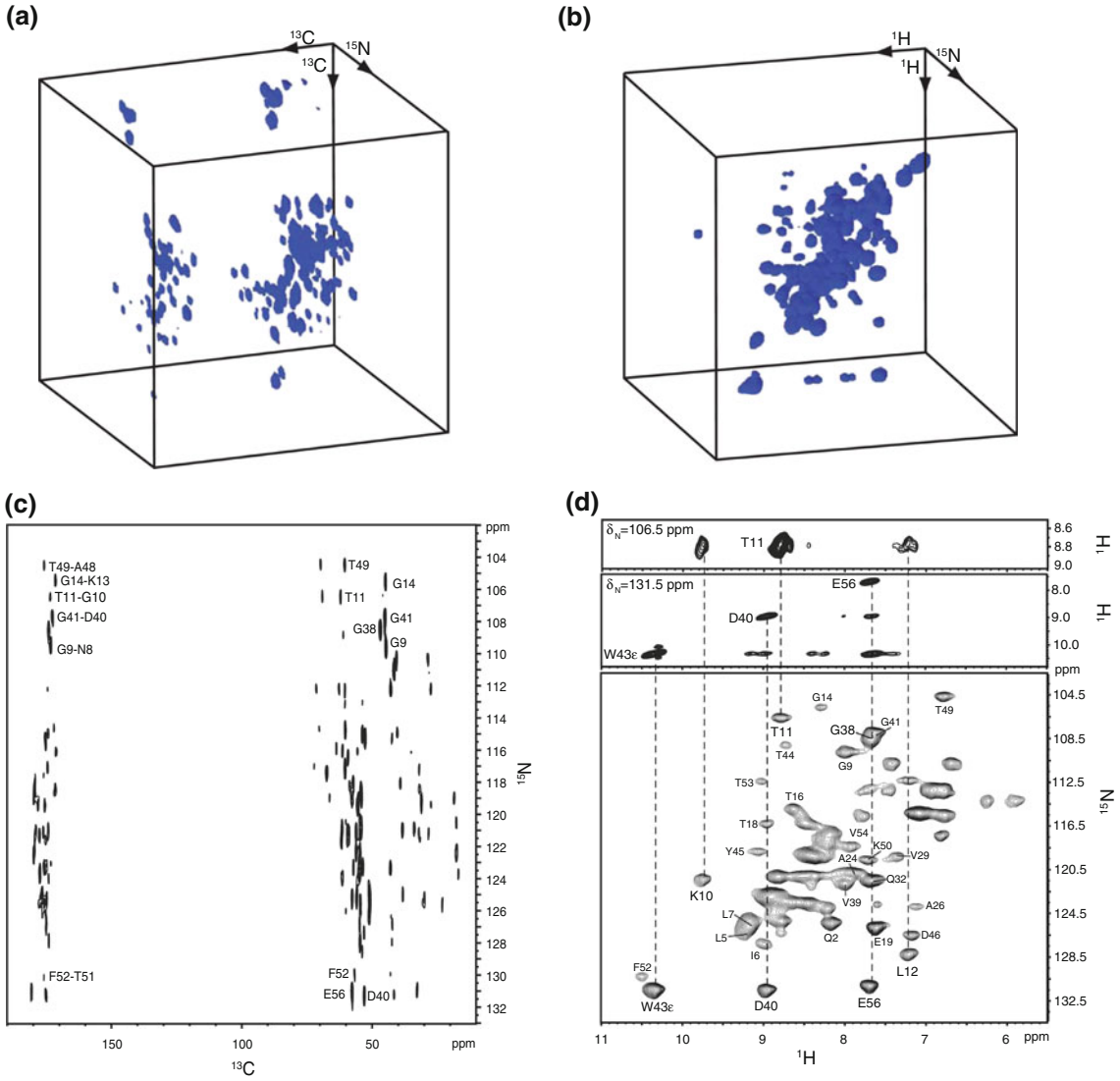

Fig. 4 Simultaneously acquired 3D NCAC (**a**) and 3D NHH (**b**) spectra of perdeuterated GB1 (NH:ND 10:90 (crystal form A)) recorded at 750 MHz and a spinning speed of 27.5 kHz. The $R16_{49}^{-5,4}$ symmetry with the corresponding numerically optimised *R* element (Fig. 1), ^{1}H–^{15}N CP contact time of 2 ms, ^{15}N–^{13}C mixing time of 3.56 ms, ^{13}C and ^{15}N RF field strength of 18 kHz during mixing, 32 transients per t_1 increment, 24 t_1 increments, 56 t_2 increments, spectral widths in the indirect dimensions of 3,000 Hz (^{15}N) and 6,036 ($^{13}CA/^{1}H$) and a recycle time of 2.0 s. The ^{1}H, ^{13}C and ^{15}N RF carriers were set to 2.5, 55 and 120 ppm, respectively. The ^{13}C RF carrier was switched to 100 ppm during ^{13}C–^{13}C mixing carried out in the absence of ^{1}H decoupling via RFDR using tanh/tan adiabatic pulses of 36.36 μs duration with $R6_6^2R6_6^{-2}$ supercycling (Brinkmann et al. 2002) for a period of ~1.7 ms and employing an RF field strength of ~70 kHz. The ^{1}H RF carrier was kept at 9.5 ppm during ^{1}H evolution in t_2 and during ^{1}H–^{1}H mixing via RFDR using tanh/tan adiabatic pulses of 20.36 ms duration with xy-16 supercycling for a period of ~4.7 ms and employing an RF field strength of ~125 kHz. ^{15}N decoupling during ^{1}H acquisition was carried out via waltz16 decoupling scheme at a power level of ~7 kHz. (**c**) $^{15}N^{13}C$ spectrum from a 2D version of the 3D experiment acquired with 128 transients per t_1 increment, 64 t_1 increments and with other parameters as mentioned above. (**d**) ^{1}H–^{1}H strips taken from the 3D NHH spectrum at the ^{15}N chemical shifts indicated. The ^{15}N–^{1}H HSQC spectrum of perdeuterated GB1 (NH:ND 10:90) collected at a spinning speed of 27.5 kHz is shown for reference. Assignments in (d) were taken from the literature (Zhou et al. 2007)

plane and subjected to a reverse CP step for transferring the magnetisaton to different spatially proximal protons for direct detection in t_3'. This approach including the optimised $R16_{49}^{-5,4}$ symmetry-based band-selective heteronuclear mixing scheme, yields satisfactory 3D NC'H and NHH spectra (Fig. 5) of a perdeuterated sample of the SH3 domain (NH:ND 30:70). It is worth emphasising that no significant signal losses were observed by keeping the ^{13}CO magnetisation in the *z* state even for a period of ~200 ms in the perdeuterated sample studied here.

The dual sequential acquisition procedure is also applicable for the collection of 3D data with ^{13}C direct

detection. For example, the RF pulse scheme (Fig. 3c) permits the simultaneous acquisition of 3D NCOC (Castellani et al. 2003; Franks et al. 2007; Schuetz et al. 2010; Sperling et al. 2010; Shi et al. 2011) and 3D CONCA (Astrof et al. 2001; Schuetz et al. 2010; Shi et al. 2011) correlation spectra for a fully protonated protein sample and resulting from the magnetisation transfer pathways $^{1}H \rightarrow {}^{15}N \rightarrow {}^{13}CO \rightarrow {}^{13}C$ and $^{1}H \rightarrow {}^{13}CO \rightarrow {}^{15}N \rightarrow {}^{13}CA$, respectively. Unlike the RF pulse scheme given in Fig. 3a, the first step in the scheme Fig. 3c involves the simultaneous generation of transverse $^{15}N/^{13}C$ magnetisations by the cross-polarisation (CP) procedure (see Herbst et al. 2008, 2010). These transverse magnetisations are allowed to evolve during the t_1/t_1' period, flipped to the

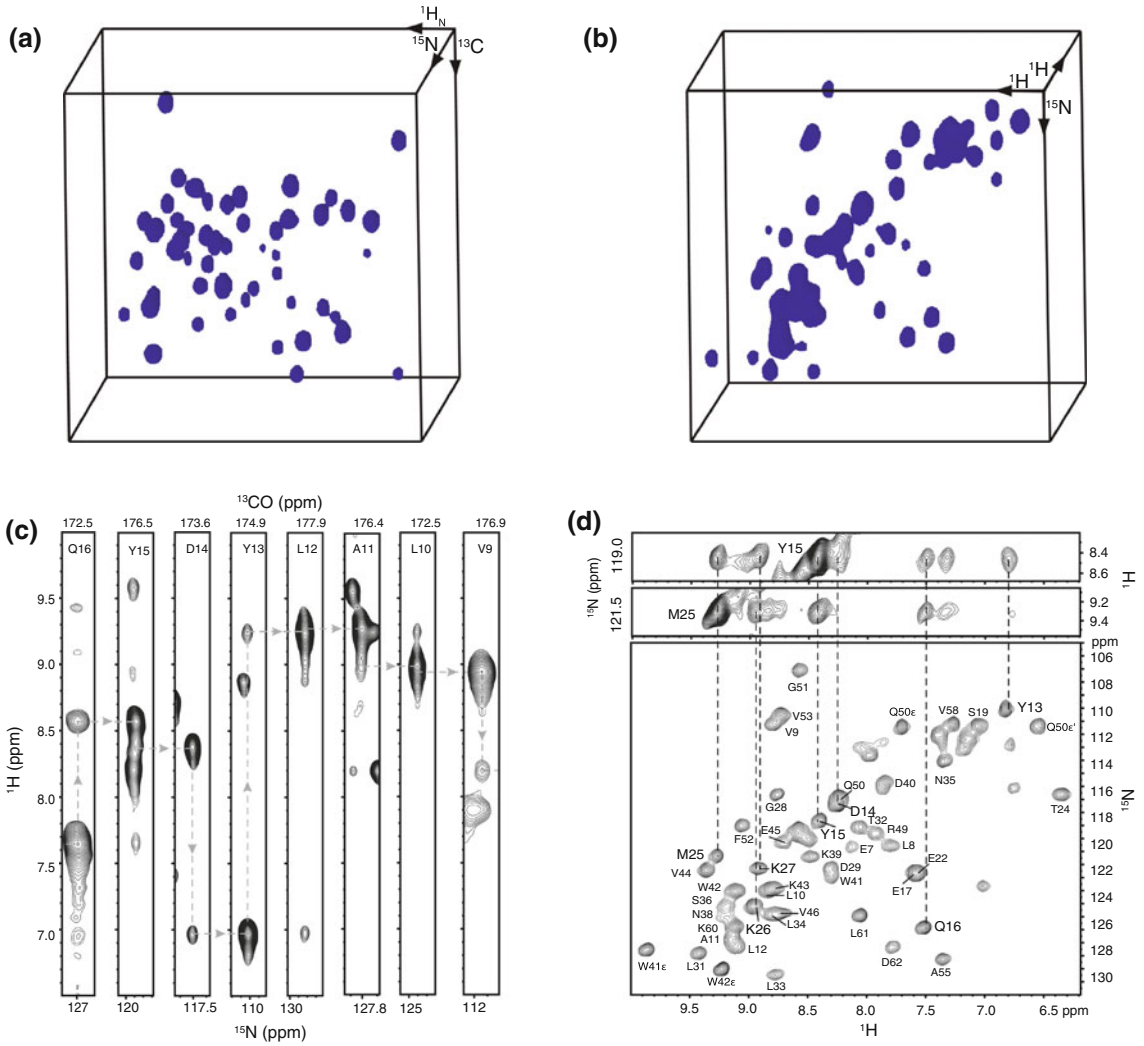

Fig. 5 Simultaneously acquired 3D NCOH (**a**) and 3D NHH (**b**) spectra of perdeuterated SH3 domain (NH:ND 30:70) recorded at 500 MHz and a spinning speed of 33.333 kHz. The $R16_{49}^{-5,4}$ symmetry with the corresponding numerically optimised *R* element, $^{1}H–^{15}N$ CP contact time of 0.5 ms, $^{1}H–^{13}C$ CP contact time of 4 ms, $^{15}N–^{13}C$ mixing time of 2.94 ms, ^{13}C and ^{15}N RF field strength of ~22 kHz during mixing, 64 transients per t_1 increment, 24 t_1 increments, 48 t_2 increments, spectral widths in the indirect dimensions of 1,500 Hz (^{15}N) and 4,000 Hz ($^{13}CO/^{1}H$) and a recycle time of 2.0 s were used, keeping the ^{1}H, ^{13}C and ^{15}N RF carriers at 9.0, 174 and 120 ppm, respectively. RFDR using tanh/tan adiabatic pulses of 20.00 μs duration with xy-16 supercycling for a period of ~7.68 ms and employing an RF field strength of ~125 kHz was employed for $^{1}H–^{1}H$ mixing. ^{15}N decoupling was carried out via the repetitive application of ^{15}N π pulses (Zhou et al. 2007) of 64 μs duration with an inter-pulse delay of 30 μs. ^{1}H decoupling during ^{15}N evolution was achieved via the repetitive application of ^{1}H π pulses of 8 μs duration with an inter-pulse delay of 30 μs. A numerically designed (Herbst et al., unpublished) phase-modulated band-selective refocussing 180° pulse of 200 μs duration was employed during the t_2' period to achieve homonuclear *J*-decoupling. (c) $^{15}N–^{1}H$ strips from the 3D NCOH spectrum taken at the ^{13}CO chemical shifts indicated. These spectra show the sequential walk along the backbone residues spanning the region Val9-Glu16. In addition to correlations arising from $CO^{i-1} \rightarrow H_N^i$ and $CO^{i-1} \rightarrow H_N^{i-1}$ magnetisation transfers, weak non-sequential correlations, e.g. due to hydrogen bonds across β-strands, are also observed. (d) $^{1}H–^{1}H$ strips taken from the 3D NHH spectrum at the ^{15}N chemical shifts indicated. The $^{15}N–^{1}H$ HSQC spectrum of perdeuterated SH3 domain (NH:ND 30:70) collected at a spinning speed of 33.333 kHz is given for reference. Assignments in (d) were taken from the literature (Lewandowski et al. 2011)

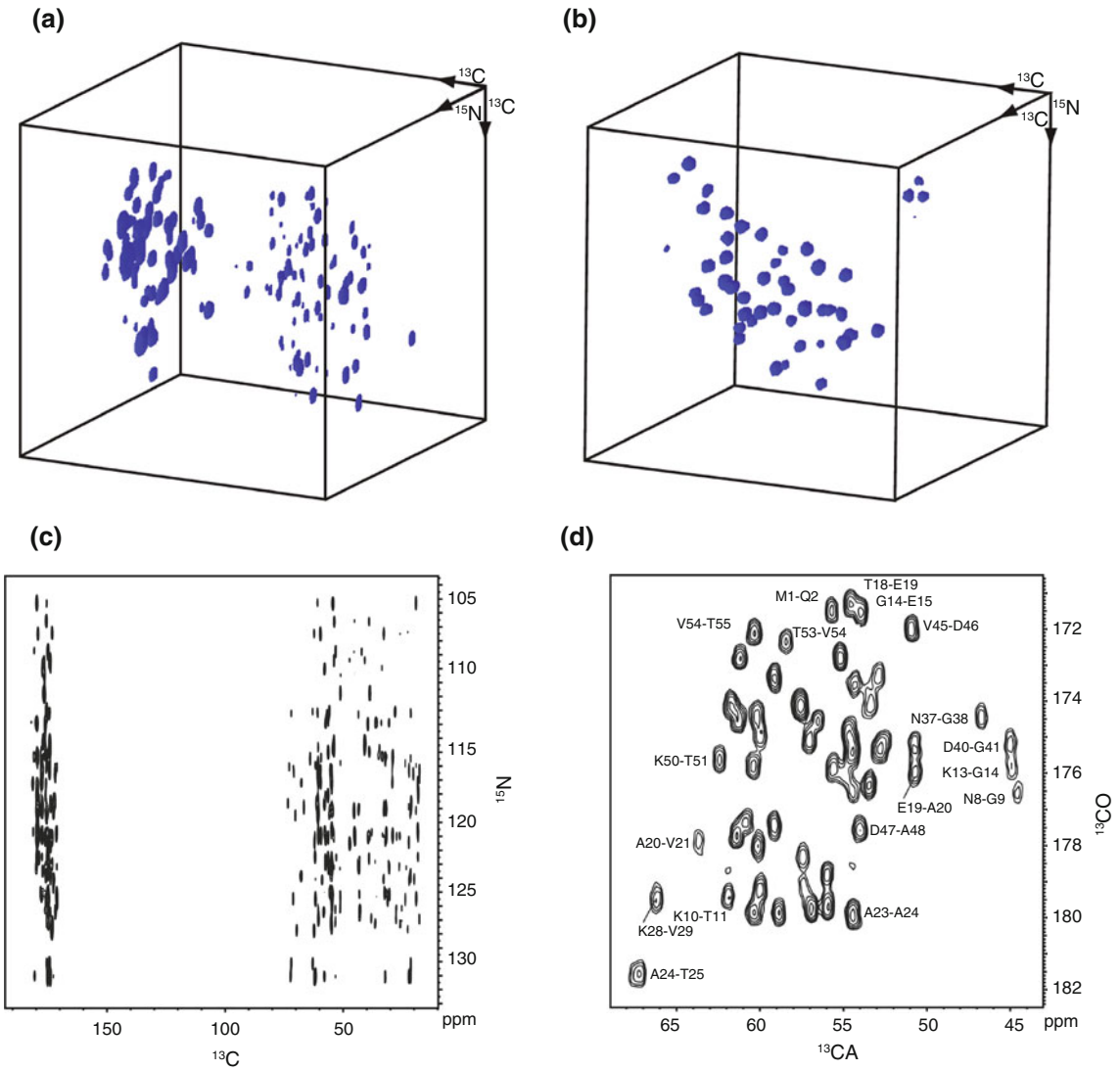

Fig. 6 Simultaneously acquired 3D NC'C (**a**) and 3D C'NCA (**b**) spectra of GB1 (crystal form A) recorded at 750 MHz and a spinning speed of 27.5 kHz. The $R16_{49}^{5,4}$ symmetry with the corresponding numerically optimised *R* element as in Fig. 1a, b, ^{1}H–^{13}C CP contact time of 1 ms, ^{1}H–^{15}N CP contact time of 1 ms, ^{15}N–^{13}C mixing time of 3.56 ms, ^{13}C and ^{15}N RF field strength of 18 kHz during mixing, 32 transients per t_1 increment, 32 t_1 increments, 48 t_2 increments, ^{15}N and ^{13}C spectral widths of 3,000 Hz in the indirect dimension and a recycle time of 2.0 s were used, keeping the ^{13}C and ^{15}N RF carriers, respectively, 175 and 120 ppm. ^{13}C–^{13}C mixing in (a) was achieved via the DARR procedure with a mixing time of 100 ms. The ^{13}C RF carrier was switched to 55 ppm at the beginning of the second ^{15}N → ^{13}C heteronuclear mixing period and switched back to 175 ppm during detection. (**c**) ^{15}N^{13}C and (d) ^{13}CO–^{13}CA spectra from a 2D version of the 3D experiment acquired with 256 transients per t_1 increment, 64 t_1 increments and with other parameters as mentioned above

z axis at the end of the evolution period and then subjected to a period of ^{15}N ↔ ^{13}CO longitudinal magnetisation exchange via the application of a band-selective symmetry-based mixing sequence. The ^{15}N/^{13}CO polarisations at the end of the heteronuclear mixing period are brought to the transverse plane and allowed to evolve during the t_2/t_2' period. The ^{15}N/^{13}CO magnetisations at the end of the evolution period are then flipped to the *z* axis. The ^{13}CO polarisation is first subjected to longitudinal homonuclear mixing during the period τ_{mix}^{CC}; e.g. via the DARR scheme (Takegoshi et al. 2001). The carbon magnetisation at the end of the mixing period is rotated back to the transverse plane and detected in t_3 to generate the 3D NCOC spectrum. After the completion of the acquisition of the first ^{13}C FID, the ^{15}N longitudinal magnetisation is then subjected to a band-selective ^{15}N → ^{13}CA longitudinal magnetisation exchange by switching the ^{13}C RF carrier frequency to the CA region. The ^{13}CA magnetisation at the end of the second heteronuclear mixing period is rotated back to the transverse plane for direct detection in t_3' to generate the 3D CONCA spectrum that provides connectivity information about two adjacent amino acid residues. After the

acquisition of the first ^{13}C FID, to minimise the effects of the residual transverse and longitudinal ^{13}C magnetisations on the ^{13}C FID collected subsequently, a sandwich of $\{\tau-(\pi/2)^{C}-\tau\}$ with $\tau = 4$ ms was applied in the absence of ^{1}H decoupling (Gopinath and Veglia 2012a, b). Eliminating signals arising from unwanted magnetisation transfer pathways via appropriate phase cycling of the RF pulses involved, this procedure allows to simultaneously acquire 3D NCOC and 3D CONCA correlation spectra (Fig. 6). The simultaneous collection of 3D NCACX and CANCO correlation spectra via dual sequential ^{13}C acquisition has also been demonstrated recently (Gopinath and Veglia 2012a).

While the 3D spectra shown in Figs. 4, 5, and 6 were generated with band-selective ^{15}N–^{13}C mixing schemes, correlation spectra resulting from ^{13}CO → ^{15}N and ^{13}CA → ^{15}N magnetisation transfer pathways can be simultaneously collected by making use of broadband mixing schemes, e.g. as shown by the RF pulse scheme (Fig. 3d) for the broadband acquisition of a 3D CNH spectrum of a protein. This RF pulse scheme has been successfully employed with a perdeuterated protein sample for the "one-shot" collection of 3D CANH (Knight et al. 2011; Ward et al. 2011) and 3D CONH (Knight et al. 2011; Ward et al. 2011) correlation spectra resulting from the magnetisation transfer pathway ^{1}H → ^{13}CA/^{13}CO → ^{15}N → ^{1}H. The initial transverse ^{13}C magnetisation is first generated by a combination of direct excitation and a cross-polarisation step (Linser 2011). It is then allowed to evolve in the absence of ^{1}H decoupling during the t_1 period. The magnetisation at the end of t_1 is flipped to the z axis and subjected to a period of ^{13}C → ^{15}N longitudinal magnetisation exchange via the application of a broadband mixing sequence. The ^{15}N polarisation generated at the end of the heteronuclear mixing period is brought to the transverse plane and allowed to evolve during the t_2 period. The magnetisation at the end of the t_2 is then flipped to the z axis. Proton saturation pulses with alternating x and y phases were then applied for 200 ms at a power level of ~30 kHz to achieve water suppression. Subsequently the ^{15}N longitudinal magnetisation is brought to the transverse plane and subjected to a CP step for transferring the magnetisaton to the directly attached proton and for direct detection in t_3. The ^{13}C RF carrier was kept near the CA region during the t_1 period and the spectral width was adjusted so as to fold the ^{13}CO resonances into the ^{13}CA spectral window. This approach including the optimised $R24_{22}^{-5,7}$ broadband heteronuclear mixing scheme (Herbst et al. 2010), yields a satisfactory 3D broadband CNH spectrum (Fig. 7) of the perdeuterated sample of the SH3 domain.

Although the acquisitions of only a few representative spectra have been demonstrated here, the approach outlined may be extended to acquire other correlation spectra. For example, with simultaneous excitation of transverse ^{15}N/^{13}C magnetisations by the first cross-polarisation step and employing dual sequential proton detection, it may be possible to achieve the simultaneous acquisition of 3D NCOH and 3D CON(H)H (Zhou et al. 2007) chemical shift correlation spectra, resulting from the magnetisation transfer pathways $^{1}H_N$ → ^{15}N → ^{13}CO → $^{1}H_N$ and $^{1}H_N$ → ^{13}CO → ^{15}N → $^{1}H_N$ ↔ $^{1}H_N$, respectively, and extract structural constraints. Dual receivers can also be employed to acquire simultaneously 3D NCC and 3D CNH correlation spectra of proteins. Broadband heteronuclear mixing sequences leading to simultaneous ^{13}CA → ^{15}N and ^{13}CO → ^{15}N magnetisation transfers can be exploited

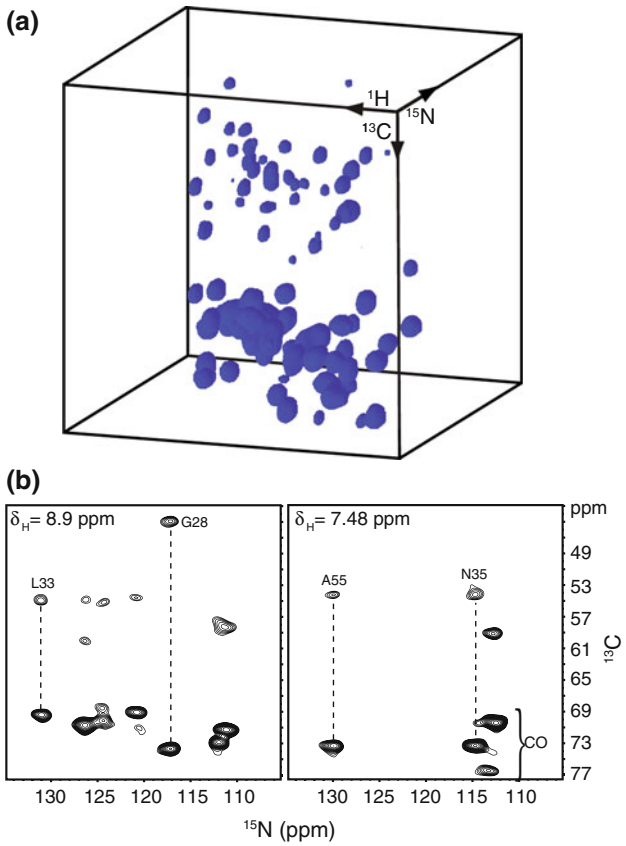

Fig. 7 3D CNH broadband chemical shift correlation spectrum (**a**) of perdeuterated SH3 domain of chicken α-spectrin (NH:ND 30:70) recorded at 500 MHz and a spinning speed of 20 kHz resulting from the magnetisation transfer pathway ^{1}H → ^{13}C → ^{15}N → ^{1}H. The $R24_{22}^{-5,7}$ symmetry with the corresponding numerically optimised R element, ^{1}H–^{13}C CP contact time of 3 ms, ^{1}H–^{15}N CP contact time of 1.5 ms, ^{15}N–^{13}C mixing time of 3.3 ms, ^{13}C and ^{15}N RF field strength of 44 kHz during mixing, 96 transients per t_1 increment, 20 t_1 increments, 32 t_2 increments, spectral widths in the indirect dimensions of 1,500 Hz (^{15}N) and 4,375 Hz (^{13}C) and a recycle time of 2.0 s. The ^{1}H, ^{13}C and ^{15}N RF carriers were set at 1, 58 and 120 ppm, respectively. The ^{13}C RF carrier was switched to 115 ppm during ^{15}N–^{13}C mixing in the absence of ^{1}H decoupling. ^{15}N decoupling in the direct dimension was carried out via the repetitive application of ^{15}N π pulses (Zhou et al. 2007) of 64 μs duration with an inter-pulse delay of 50 μs. (**b**) ^{13}C–^{15}N strips taken from the 3D CNH spectrum at the ^{1}H chemical shifts indicated

for the 3D DQ(CACO)NH-type of experiments reported recently (Ward et al. 2011). The approach outlined here for the simultaneous acquisition of multidimensional 3D data sets may also be combined with other approaches; e.g. sparse sampling in the indirect dimension, for further reducing the data acquisition times. In summary, the results presented demonstrate that it is possible to effectively use, even at high MAS frequencies, numerically designed high-power broadband and low-power band-selective homo- and heteronuclear symmetry-based mixing sequences and to achieve, with dual receivers, sequential acquisitions and broadband ^{15}N–^{13}C mixing schemes, the simultaneous acquisition of 3D correlation spectra of high quality and of interest in protein structural studies.

Acknowledgments The FLI is a member of the Science Association'Gottfried Wilhelm Leibniz' (WGL) and is financially supported by the Federal Government of Germany and the State of Thuringia. Also thanks to the Leibniz Graduate School on Aging and Age-Related Diseases (LGSA) for funding and support.

References

Agarwal V, Linser R, Fink U, Faelber K, Reif B (2010) Identification of hydroxyl protons, determination of their exchange dynamics and characterisation of hydrogen bonding in a microcrystallin protein. J Am Chem Soc 132:3187–3195

Akbey U, Lange S, Franks WT, Linser R, Rehbein K, Diehl A, Rossum BJ, Reif B, Oschkinat O (2010) Optimum levels of exchangeable protons in perdeuterated proteins for proton detection in MAS NMR spectroscopy. J Biomol NMR 46:67–73

Astrof NS, Lyon CE, Griffin RG (2001) Triple resonance solid state NMR experiments with reduced dimensionality evolution periods. J Magn Reson 152:303–307

Bennett AE, Rienstra CM, Griffiths JM, Zhen W, Lansbury PT, Griffin RG (1998) Homonuclear radio frequency-driven recoupling in rotating solids. J Chem Phys 108:9463–9479

Brinkmann A, Levitt M (2001) Symmetry principles in the nuclear magnetic resonance of spinning solids: heteronuclear recoupling by generalized Hartmann-Hahn sequences. J Chem Phys 115: 357–384

Brinkmann A, Schmedt auf der Günne J, Levitt MH (2002) Homonuclear zero-quantum recoupling in fast magic-angle spinning nuclear magnetic resonance. J Magn Reson 156:79–96

Castellani F, van Rossum BJ, Diehl A, Rehbein K, Oschkinat H (2003) Determination of solid-state NMR structures of proteins by means of three-dimensional 15 N–13C–13C dipolar correlation spectroscopy and chemical shift analysis. Biochemistry 42:11476–11483

Chen L, Kaiser JM, Lai J, Polenova T, Yang J, Rienstra CM, Mueller LJ (2007) *J*-based 2D homonuclear and heteronuclear correlation in solid-state proteins. Magn Reson Chem 45:S84–S92

Franks WT, Zhou DH, Wylie BJ, Money BG, Graesser DT, Frericks HL, Sahota G, Rienstra CM (2005) Magic-angle spinning solid-state NMR spectroscopy of the β1 immunoglobulin binding domain of protein G (GB1): ^{15}N and ^{13}C chemical shift assignments and conformational Analysis. J Am Chem Soc 127:12291–12305

Franks WT, Kloepper KD, Wylie BJ, Rienstra CM (2007) Four-dimensional heteronuclear correlation experiments for chemical shift assignments of solid proteins. J Biomol NMR 39: 107–131

Frericks Schmidt HL, Sperling LJ, Gao YG, Wylie BJ, Boettcher JM, Wilson SR, Rienstra CM (2007) Crystal polymorphism of protein GB1 examined by solid-state NMR spectroscopy and X-ray diffraction. J Phys Chem B 111:14362–14369

Gopinath T, Veglia G (2012a) Dual acquisition magic-angle solid-state NMR-spectroscopy: simultaneous acquisition of multidimensional spectra of biomacromolecules. Angew Chem Int Ed 51:1–6

Gopinath T, Veglia G (2012b) 3D DUMAS: simultaneous acquisition of three-dimensional magic angle spinning solid-state NMR experiments of proteins. J Magn Reson 220:79–84

Habenstein B, Wasmer C, Bousset L, Sourigues Y, Schutz A, Loquet A, Meier BH, Melki R, Böckmann A (2011) Extensive de novo solid-state NMR assignments of the 33 kDa C-terminal domain of the Ure2 prion. J Biomol NMR 51:235–243

Herbst C, Riedel K, Ihle Y, Leppert J, Ohlenschläger O, Görlach M, Ramachandran R (2008) MAS solid state NMR of RNAs with multiple receivers. J Biomol NMR 41:121–125

Herbst C, Herbst J, Kirschstein A, Leppert J, Ohlenschläger O, Görlach M, Ramachandran R (2009a) Design of high-power, broadband 180° pulses and mixing sequences for fast MAS solid state chemical shift correlation NMR spectroscopy. J Biomol NMR 43:51–61

Herbst C, Herbst J, Kirschstein A, Leppert J, Ohlenschläger O, Görlach M, Ramachandran R (2009b) Recoupling and decoupling of nuclear spin interactions at high MAS frequencies: numerical design of CN_n^{ν} symmetry-based RF pulse schemes. J Biomol NMR 44:175–184

Herbst C, Herbst J, Leppert J, Ohlenschläger O, Görlach M, Ramachandran R (2009c) Numerical design of RN_n^{ν} symmetry-based RF pulse schemes for recoupling and decoupling of nuclear spin interactions at high MAS frequencies. J Biomol NMR 44:235–244

Herbst C, Herbst J, Leppert J, Ohlenschläger O, Görlach M, Ramachandran R (2010) Broadband 15N–13C dipolar recoupling via symmetry-based RF pulse schemes at high MAS frequencies. J Biomol NMR 47:7–17

Herbst C, Herbst J, Leppert J, Ohlenschläger O, Görlach M, Ramachandran R (2011) Chemical shift correlation at high MAS frequencies employing low-power symmetry-based mixing schemes. J Biomol NMR 50:277–284

Hou G, Yan S, Sun S, Han Y, Byeon IL, Ahn J, Concel J, Samoson A, Gronenborn AM, Polenova T (2010) Spin diffusion driven by R-symmetry sequences: applications to homonuclear correlation spectroscopy in MAS NMR of biological and organic solids. J Am Chem Soc 133:3943–3953

Huang KY, Siemer AB, McDermott AE (2011) Homonuclear mixing sequences for perdeuterated proteins. J Magn Reson 208: 122–127

Kehlet C, Bjerring M, Sivertsen AC, Kristensen T, Enghild JJ, Glaser SJ, Khaneja N, Nielsen NC (2007) Optimal control based NCO and NCA experiments for spectral assignments in biological solid-state NMR spectroscopy. J Magn Reson 188:216–230

Knight MJ, Webber AL, Pell AJ, Guerry P, Barbet-Massin E, Bertini I, Felli IC, Gonnelli L, Pierattelli R, Emsley L, Lesage A, Herrmann T, Pintacuda G (2011) Fast resonance assignment and fold determination of human superoxide dismutase by high-resolution proton-detected solid-state MAS NMR spectroscopy. Angew Chem Int Ed 50:11697–11701

Leppert J, Heise B, Ohlenschläger O, Görlach M, Ramachandran R (2003) Broadband RFDR with adiabatic inversion pulses. J Biomol NMR 26:13–24

Levitt MH (2002) Symmetry-based pulse sequences in magic-angle spinning solid-state NMR. In: Grant DM, Harris RK (eds) Encyclopedia of nuclear magnetic resonance. Wiley, Chichester

Lewandowski JR, Dumaz JN, Akbey U, Lange S, Emsley L, Oschkinat H (2011) Enhanced resolution and coherence lifetimes in the solid-state NMR spectroscopy of perdeuteraded proteins under ultrafast magic-angle spinning. J Phys Chem Lett 2: 2205–2211

Linser R (2011) Side-chain to backbone correlations from solid-state NMR of perdeuterated proteins through combined excitation and long-range magnetization transfers. J Biomol NMR 51:221–226

Linser R (2012) Backbone assignment of perdeuterated proteins using long-range H/C transfers. J Biomol NMR 52:151–158

Linser R, Bardiaux B, Higman V, Fink U, Reif B (2011) Structure calculation from unambiguous long-range amide and methyl 1H–1H distance restraints for a microcrystalline protein with MAS solid-state NMR spectroscopy. J Am Chem Soc 133: 5905–5912

Loening NM, Bjerring M, Nielsen NC, Oschkinat H (2012) A comparison of NCO and NCA transfer methods for biological solid-state NMR spectroscopy. J Magn Reson 214:81–90

Nielsen AB, Bjerring M, Nielsen JT, Nielsen NC (2009) Symmetry-based dipolar recoupling by optimal control: band-selective experiments for assignment of solid-state NMR spectra of proteins. J Chem Phys 131:025101

Paulson EK, Morcombe CR, Gaponenko V, Dancheck B, Byrd RA, Zilm KW (2003) High-sensitivity observation of dipolar exchange and NOEs between exchangeable protons in proteins by solid-state NMR spectroscopy. J Am Chem Soc 125: 14222–14223

Schuetz A, Wasmer C, Habenstein B, Verel R, Greenwald J, Reik R, Böckmann A, Meier BH (2010) Protocols for the sequential solid-state NMR spectroscopic assignments of a uniformly labeled 25 kDa protein:HET-s(1–227). ChemBioChem 11: 1543–1551

Shi L, Kawamura I, Jung KH, Brown LS, Ladizhansky V (2011) Conformation of a seven- helical transmembrane photosensor in the lipid environment. Angew Chem Int Ed 50:1302–1305

Sperling LJ, Berthold DA, Sasser TL, Jeisy-Scott V, Rienstra CM (2010) Assignments strategies for large proteins by magic-angle spinning NMR: the 21-kDa disulfide-bond forming enzyme Dsba. J Mol Biol 399:268–282

States DJ, Haberkorn RA, Ruben DJ (1982) A two-dimensional nuclear Overhauser experiment with pure absorption phase in four quadrants. J Magn Reson 48:286–292

Takegoshi K, Nakamura S, Terao T (2001) 13C–1H dipolar-assisted rotational resonance in magic-angle spinning NMR. Chem Phys Lett 344:631–637

Ward ME, Shi L, Lake E, Krishnamurthy S, Hutchins H, Brown LS, Ladizhansky V (2011) Proton-detected solid-State NMR reveals intramembrane polar networks in a seven-helical transmembrane protein proteorhodopsin. J Am Chem Soc 133:17434–17443

Zhou DH, Rienstra CM (2008) High-performance solvent suppression for proton detected solid- state NMR. J Magn Reson 192: 167–172

Zhou DH, Shea JJ, Nieuwkoop AJ, Franks WT, Wylie BJ, Mullen C, Sandoz D, Rienstra CM (2007) Solid-State Protein-Structure Determination with Proton-Detected Triple-Resonance 3D Magic-Angle-Spinning NMR Spectroscopy. Angew Chem Int Ed 46:8380–8383